The influence of low-temperature argon matrix on embedded water clusters. A DFT theoretical study

A. Vasylieva[1], I. Doroshenko[1], S. Stepanian[2], and L. Adamowicz[3, 4]

[1]Taras Shevchenko National University of Kyiv, Kyiv 01601, Ukraine
E-mail: an.vasylieva@gmail.com

[2]B. Verkin Institute for Low Temperature Physics and Engineering of the National Academy of Sciences of Ukraine
Kharkiv 61103, Ukraine

[3]Department of Chemistry and Biochemistry, University of Arizona, Tucson AZ 85721, USA

[4]Interdisciplinary Center for Modern Technologies, Nicolaus Copernicus University
Toruń PL 87-100, Poland

Computer simulations of an argon fcc crystal fragment with embedded water clusters of different sizes are performed using the quantum mechanical DFT/M06-2X method. The effect of the argon matrix on the structural, energy, and spectral parameters of individual water clusters are investigated. The formation energies of $(H_2O)_n@Ar_m$ complexes, as well as deformation energies of water clusters and of the argon crystal involved in the embedment, are computed for $n = 1$–7. Matrix shifts of the IR vibrational frequencies of water clusters isolated in argon matrices are predicted based on the results of the calculations. The predictions indicate a possibility of the formation of small stable water complexes in low-temperature argon matrices.

Keywords: IR spectroscopy, low-temperature matrix isolation, argon, water clusters, DFT/M06-2X calculations.

1. Introduction

The vibrational spectra of water isolated in a low-temperature inert matrix are similar to the spectra of water in the gas phase. However, numerous results of experimental studies of water show some differences in the position of the spectral bands in the matrix compared to the gas phase [1–9]. This indicates that the solid inert matrix influences the structural and energy characteristics of the water clusters isolated in the matrix [10, 11].

The advantage of using an inert matrix medium is the weak interaction of the studied molecule with the surrounding environment. Nevertheless, when water molecules get into nanosize cavities (vacancies) in the matrix crystal, an influence of the cavity walls on their structure and behavior appears and affects the molecules. The inert matrix has a relatively weak interaction with the molecules trapped in it. This interaction is equal to about 1 kcal/mol (4–5 kJ/mol) per atom of the matrix-isolated molecule [4]. Such interaction can usually be neglected. Although argon is an inert medium, it was noted in [3] that a molecule trapped in the lattice of a solid-state matrix interacts with the surrounding argon atoms with forces characteristic to atom-molecule interactions. The peculiarities of the interactions of the "guest" molecules and the "host" matrix were studied by methods of supramolecular chemistry in the framework of the microsolubility theory [3].

A comparison of the experimentally recorded IR absorption spectra of water isolated in an argon matrix with the water spectra obtained in the gas phase allows to determine the vibrational frequencies shifts. According to [4, 10, 12], in the IR spectra of matrix-isolated molecules, in addition to the matrix shifts of the spectral bands of the molecules, additional bands may appear. This is due to the so-called matrix splitting, which results from different ways of embedding of hydrogen-bonded clusters in the matrix cavities. The interaction of the matrix sites with labile water clusters isolated in them can also lead to a change in the structure of hydrogen-bonded aggregates, which, in turn, can cause significant changes in the IR spectrum of water [12]. These matrix effects may be related to the influence of different symmetries of the matrix vacancies and the dielectric

constant of the matrix medium, as well as to the ability of the water OH groups to form weak hydrogen bonds with the atoms of the matrix [3, 4, 10, 13].

Quantum-chemical simulation can be useful to elucidate the influence of the solid matrix on the species trapped in it. An attempt to determine the influence of the argon environment on the isolated water clusters was made in [6] with simulations of the vibrational spectra of the water clusters embedded in a continuous argon environment. A comparison of the results of the calculations with the experimental data showed that the calculated shifts of the spectral bands corresponding to both the stretching and bending OH vibrations are smaller than the shifts observed in the experiment [6]. A more accurate approach to investigate the matrix effects is to construct a model of the crystal lattice of the inert-gas atoms, in which a certain number of the lattice atoms in the center of the crystal fragment is replaced by the "guest" molecule. For such a model, quantum-chemical calculations can be performed to determine the optimal structure of the complex formed by the "guest" molecules with the surrounding matrix and the corresponding vibrational spectrum. The approach was used to investigate the effects of low-temperature matrices on the IR absorption spectra of small molecules [10, 11, 14, 15]. In the present work, the DFT/M06-2X method is used to estimate the effects of argon matrices on the structure, relative stabilities, and vibrational frequencies of embedded water clusters. The considered water cluster is $(H_2O)_n$ with $n = 1–7$.

2. Computational details

In the simulation of the matrix-isolation experiment, fragments of argon face-centered cubic (fcc) crystal with one or more Ar atoms substituted with different numbers of water molecules are used. Such model systems are denoted as $(H_2O)_n@Ar_m$, where n is the number of water molecules in the cluster and m is the number of argon atoms in the crystal fragment. For example, for a water monomer embedded in a crystal fragment comprising of 108 argon atoms, two model matrix fragments with one and two Ar atoms substituted by the water molecule are considered. These fragments are denoted as $H_2O@Ar_{107}$ and $H_2O@Ar_{106}$. The $(H_2O)_2@Ar_{106}$ complex is used to simulate a water dimer embedded in the matrix, and substituting two argon atoms. In the same way, model matrix fragments containing larger clusters of water molecules are formed. For larger water clusters embedded in fcc argon fragments, some different possible embedding configurations are considered. The simulations include ring and chain water clusters (with $n = 3–5$), as well as for four isomers for the hexamer water cluster and one isomer for the heptamer water cluster. In the simulations of the embedded water clusters with $n \geq 5$, we use a larger matrix fragment consisting of 171 argon atoms. The geometry optimizations and harmonic frequency calculations are performed with the DFT method using the M06-2X functional [16]. The standard aug-cc-pVDZ basis set is used

for the water molecules and the CRENBL ECP (effective core potential) [17–19] is used for the argon atoms. All quantum-mechanical calculations are performed using the Gaussian 16 program package [20].

3. Results and discussion

3.1. Interaction energies between argon matrix environment and the water clusters

The optimized structures of the water monomer, dimer, ring trimer, and ring tetramer embedded in argon fcc crystals are shown in Fig. 1.

The size and shape of the matrix site, where a water cluster is embedded, primarily depend on the structure of the embedded cluster [10, 12]. To determine the size of the matrix site and the number of argon atoms that need to be removed to make room for the water cluster, additional calculations of molar volumes of the studied water clusters and of an argon atom are performed (see Table 1). The volume is estimated using a spherical cavity with the electron density inside the cavity being greater than 0.001 electrons/a_0^3. According to [4], such estimation, which is based on the ratio of the volume of the embedded water cluster and the volume of the displaced argon atoms, provides only the minimum size of the matrix cavity. In a more precise evaluation of the cavity volume, one should also take into account the shape of the embedded water cluster. For example, in [12], the shape of the matrix cavity for a formic acid molecule was determined by performing a molecular dynamics calculation. In the present work, the calculations of the shape of the matrix cavity are not performed due to the relatively small sizes of the water clusters.

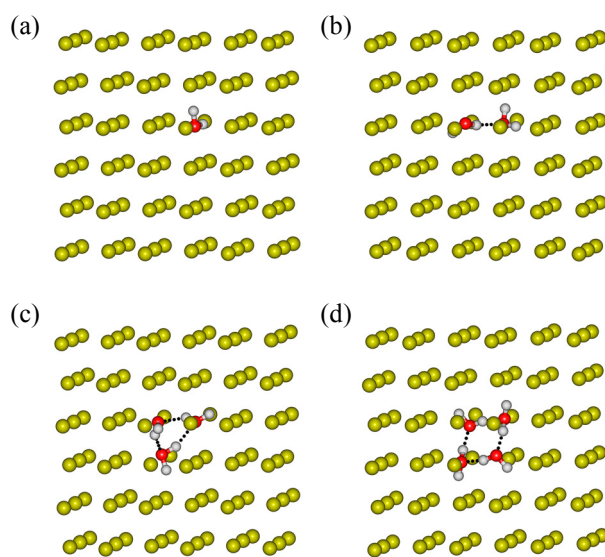As can be seen from Table 1, the volume of the water monomer is approximately equal to the volume of an argon

Fig. 1. (Color online) Structures of the $H_2O@Ar_{107}$ (a), $(H_2O)_2@Ar_{106}$ (b), $(H_2O)_3@Ar_{104}$ (c), and $(H_2O)_4@Ar_{104}$ (d) clusters calculated using the DFT/M06-2X method.

Table 1. The calculated values of molar volumes of optimized water clusters structures. The Bohr radius is $a_0 = 0.52918$ Å

Structure	V, a_0^3/mol	V, Å^3/mol
H_2O	218	32
$(H_2O)_2$	431	64
$(H_2O)_3$	411	61
$(H_2O)_4$	718	106
$(H_2O)_5$	838	124
$(H_2O)_6^{ring}$	1078	160
$(H_2O)_6^{combo}$	902	134
$(H_2O)_6^{cage}$	906	134
$(H_2O)_6^{prism}$	1066	158
$(H_2O)_7^{prism}$	1099	163
Ar	243	36

atom. It means that, to make room in the matrix for one embedded water molecule, only one Ar atom needs to be removed. However, for the sake of generality, in addition to the simulation of the $H_2O@Ar_{107}$ complex, a simulation of the $H_2O@Ar_{106}$ complex that contains one fewer Ar atom is performed. For the water dimer, the simulation is done for the $(H_2O)_2@Ar_{106}$ complex where the water dimer replaces two argon atoms. For the water trimer, several options for the embedding in the Ar matrix are considered. These are $(H_2O)_3@Ar_{105}$ and $(H_2O)_3@Ar_{104}$ for the ring trimer, and $(H_2O)_3@Ar_{105}^{linear}$ for the chain trimer. The optimized structures of the complexes are shown in Fig. 2(a). For the ring water tetramer, the simulations are performed for two complexes, $(H_2O)_4@Ar_{104}$ [Fig. 1(d)] and $(H_2O)_4@Ar_{103}$, as well as for one complex for the chain tetramer, $(H_2O)_4@Ar_{104}^{linear}$ [Fig. 2(b)]. For the water pentamer, the simulations of the embedding into the argon matrix include two water clusters, a water cluster in the form of a ring, $(H_2O)_5@Ar_{166}$, and a chain cluster, $(H_2O)_5@Ar_{166}^{linear}$. For larger water clusters isolated in the argon matrix fragment, the simulations are performed for four hexamer isomers, $(H_2O)_6@Ar_{164}^{ring}$, $(H_2O)_6@Ar_{163}^{cage}$, $(H_2O)_6@Ar_{163}^{prism}$, and $(H_2O)_6@Ar_{163}^{combo}$, and one heptamer isomer, $(H_2O)_7@Ar_{162}^{prism}$. The optimized geometries of some of these clusters are presented in Fig. 3.
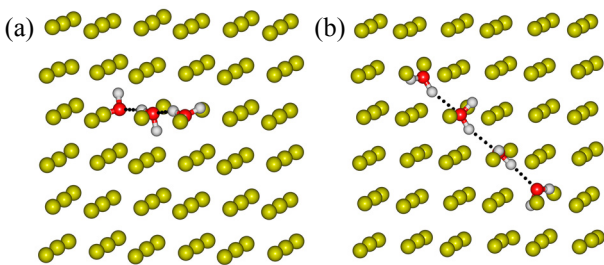

Fig. 2. (Color online) Optimized structures of the $(H_2O)_3@Ar_{105}^{linear}$ (a) and $(H_2O)_4@Ar_{104}^{linear}$ (b) clusters calculated using the DFT/M06-2X method.
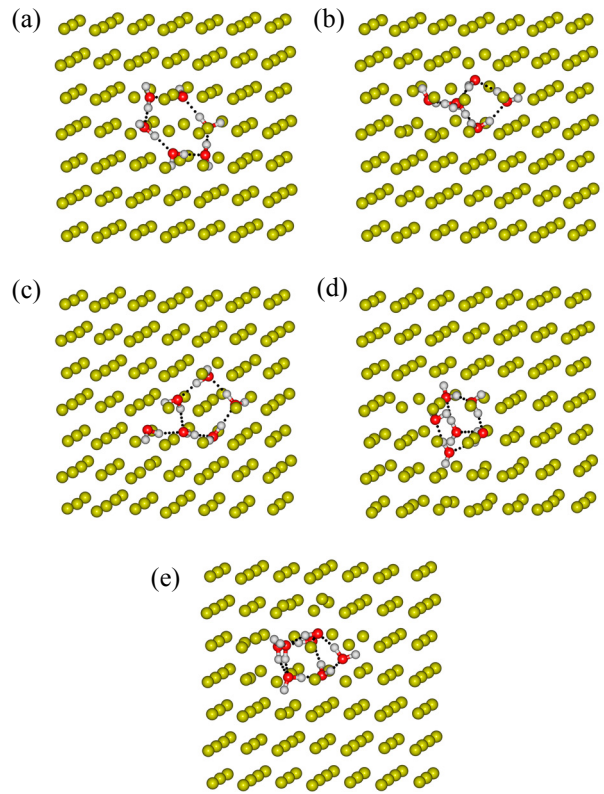

Fig. 3. (Color online) Optimized structure of the $(H_2O)_6@Ar_{164}^{ring}$ (a), $(H_2O)_6@Ar_{163}^{cage}$ (b), $(H_2O)_6@Ar_{163}^{combo}$ (c), $(H_2O)_6@Ar_{163}^{prism}$ (d), and $(H_2O)_7@Ar_{162}^{prism}$ (e) clusters calculated using the DFT/M06-2X method.

According to [4, 10, 12], the need to consider the incorporation of hydrogen-bonded water clusters into matrix sites of a larger size is due to the fact that in the process of forming an inert matrix at temperatures significantly below the melting point of argon, matrix encapsulation, which do not correspond to the global energy minimum of the embedded molecular structures, can be formed. When the temperature of the matrix is increased, the matrix cavities can transform, which is accompanied with the embedded hydrogen-bonded clusters assuming more energetically favorable configurations [12].

To find the optimal geometries of the two individual components of the complex, the structures of both the water cluster and the argon crystal are optimized separately. The optimization of the geometry of the water cluster is performed starting from the optimization with the cluster structures before the incorporation of the cluster into the crystal cavity and after the incorporation, the optimized structure with the lowest energy is used to analyze the changes of the structural and energy parameters. In the calculation of the interaction energy, E_{int}, of the fragment of an inert-gas crystal with a trapped water cluster, the standard counterpoise correction approach is used [21].

During the incorporation of water clusters into the matrix, deformation of the structures of both the water clusters and the inert-gas crystal is observed. The cluster de-

formation energy, E_{def}, can be calculated as the difference between the energy of the free water cluster in its optimal configuration and the energy of its configuration when the cluster is embedded in the matrix fragment [10]. Similarly, the deformation energy of the matrix fragment can be calculated as the difference between the energy of the fragment in the optimal configuration and the energy of its configuration in the complex. The latter two energies are calculated for the fragment where the water cluster is removed but not replaced with the Ar atoms.

The energy of the complex formation, E_{form}, is calculated as the sum of the interaction energy, the deformation energy of the water complex, and the deformation energy of the matrix fragment [10]:

$$E_{form} = E_{int} + (E_{def}^{clast} + E_{def}^{cryst}).$$

The interaction energy, E_{int}, the deformation energy, E_{def}, and the formation energy, E_{form}, allow to estimate the stability of the water cluster before and after it is embedded in the matrix [12]. The calculated energy values for all simulated complexes, $(H_2O)_n@Ar_m$, are shown in Tables 2 and 3.

Analysis of the deformation energies of the embedded water clusters allows us to note that the largest energy changes occur for the chain structures (see Tables 2 and 3). For the chain trimer, tetramer, and pentamer, the deforma-

tion energies are 28.9, 57.3, and 77.4 kJ/mol, respectively. This was to be expected because, in the absence of the matrix environment, the most energetically favorable geometry of a cluster water cluster with the number of the water molecules from 3 to 5 is circular [2]. Thus, as mentioned, the energy of the circular cluster is used in the calculation of the deformation energies of both the chain and circular clusters embedded in the matrix.

According to Table 2, the deformation energy of the monomer, dimer, and ring trimer is rather small and ranges from 0.02 to 4.2 kJ/mol. For complexes with water monomer, similar values of the total deformation energy, $E_{def}^{clast} + E_{def}^{cryst}$, are obtained for $H_2O@Ar_{107}$ (0.7 kJ/mol) and for $H_2O@Ar_{106}$ (1.12 kJ/mol) with the deformation energy for $H_2O@Ar_{106}$ being slightly higher. It means that an increase in the matrix cavity size for the monomer leads to an increase in the deformation energy. The complex formation energy is –16.7 kJ/mol, which is 2.5 kJ/mol lower than the formation energy of the $H_2O@Ar_{106}$ complex. According to the results of the calculations, smaller values of the deformation energies of the crystal and the water molecule and a higher absolute value of the formation energy are obtained by replacing one argon atom in the crystal fragment by a water molecule and formation of the $H_2O@Ar_{107}$ complex. Thus, according to the calculations, the formation of the $H_2O@Ar_{107}$ complex is more energetically favorable than the $H_2O@Ar_{106}$ complex.

For the water dimer, one structure of the $(H_2O)_2@Ar_{106}$ complex is considered. The deformation energy of the water cluster in this complex is 0.3 kJ/mol and the total deformation energy is 4.6 kJ/mol. The formation energy is –31.0 kJ/mol. Among the considered complexes with the ring water trimer, the lowest total deformation energy of 2.3 kJ/mol is obtained for the $(H_2O)_3@Ar_{104}$ complex, but the lowest formation energy is obtained for the $(H_2O)_3@Ar_{105}$ complex. According to the data in Table 3, between the two considered embedded ring tetramers, the $(H_2O)_4@Ar_{103}$ complex shows less deformation, but lower formation energy is obtained for the $(H_2O)_4@Ar_{104}$ complex (–44.7 kJ/mol).

Among the considered embedded isomers of the water hexamer, the smallest total deformation of the system is observed for the complexes with the ring hexamer, $(H_2O)_6@Ar_{164}$ (8.0 kJ/mol), and with the prism hexamer, $(H_2O)_6@Ar_{163}^{prism}$ (10.6 kJ/mol). The formation energies of these two complexes are –55.0 and –52.8 kJ/mol, respectively. The lowest formation energy of –63.6 kJ/mol is obtained for the $(H_2O)_6@Ar_{164}^{combo}$ complex.

It is interesting that the lowest deformation energy of the water hexamer cluster of 0.002 kJ/mol is observed for the "cage"-type isomer, but at the same time, the deformation energy of the argon crystal of 24.5 kJ/mol is the highest for this complex. According to the results of the calculations, the embedding of the "cage" hexamer in the Ar matrix fragment with 163 Ar atoms causes the largest deformation of the fcc matrix fragment.

Table 2. The calculated interaction energy, E_{int}, deformation energy, E_{def}, and formation energy, E_{form}, for the $(H_2O)_n@Ar_m$, $n = 1–3$, complexes

Complex	E_{int}, kJ/mol	E_{def}, kJ/mol		E_{form}, kJ/mol
		Ar	$(H_2O)_n$	
$H_2O@Ar_{107}$	–16.0	0.6	0.1	–16.7
$H_2O@Ar_{106}$	–13.0	1.1	0.02	–14.2
$(H_2O)_2@Ar_{106}$	–26.4	4.3	0.3	–31.0
$(H_2O)_3@Ar_{105}$	–33.2	3.1	0.8	–37.1
$(H_2O)_3@Ar_{104}$	–32.9	1.7	0.6	–35.3
$(H_2O)_3@Ar_{105}^{linear}$	–10.4	1.5	28.9	20.0

Table 3. The calculated interaction energy, E_{int}, deformation energy, E_{def}, and formation energy, E_{form}, for the $(H_2O)_n@Ar_m$ complexes with $n = 4–7$

Complex	E_{int}, kJ/mol	E_{def}, kJ/mol		E_{form}, kJ/mol
		Ar	$(H_2O)_n$	
$(H_2O)_4@Ar_{104}$	–36.5	6.7	1.5	–44.7
$(H_2O)_4@Ar_{103}$	–35.9	3.4	1.6	–40.8
$(H_2O)_4@Ar_{104}^{linear}$	11.5	5.1	57.3	–50.9
$(H_2O)_5@Ar_{166}$	–16.8	22.4	2.4	–41.6
$(H_2O)_5@Ar_{166}^{linear}$	18.2	4.1	77.4	–63.3
$(H_2O)_6@Ar_{164}$	–47.0	2.4	5.6	–55.0
$(H_2O)_6@Ar_{163}^{cage}$	–24.9	24.5	0.002	–49.4
$(H_2O)_6@Ar_{163}^{prism}$	–42.3	6.5	4.1	–52.8
$(H_2O)_6@Ar_{164}^{combo}$	–44.7	7.6	11.3	–63.6
$(H_2O)_7@Ar_{162}^{prism}$	–18.9	26.2	4.2	–49.4

For the water heptamer cluster embedded in the fragment of the argon crystal, the deformation energy of the cluster is 4.2 kJ/mol, while the deformation energy of the crystal is significant and approximately equal to 26.2 kJ/mol. The formation energy of the $(H_2O)_7@Ar_{162}^{prism}$ complex is equal to –49.4 kJ/mol.

Thus, the analysis of the energy parameters of the complexes considered above allows us to conclude that the most energetically favorable are complexes of the matrix fragment with a small number of water molecules. An additional information on the formation of water complexes in the argon matrix comes from comparing the frequency matrix shift in the calculated spectra with the experimental spectra.

3.2. Changes in the structure of water clusters embedded in the fragment of an argon crystal

In addition to the analysis of the energy parameters of the complexes formed by water clusters with fragments of the Ar matrix, the influence of the matrix environment on the structural parameters of the embedded water clusters is worth investigating. Such analysis can show how the structures of the clusters are changed due to the interaction with the matrix environment.

An analysis of changes in the structural parameters of the water clusters shows that the largest changes occur in the geometries of the chain structures. According to the calculated energy parameters presented above, the chain structures outside the matrix are the least energetically favorable and have the highest deformation energies when embedded in the Ar matrix.

Let us consider the structural changes that occur in the cyclic water clusters upon embedding them in the matrix. The changes are evaluated for the monomer, dimer, and cyclic clusters containing from 3 to 6 water molecules. The changes in such structural parameters as the angle of the water molecules ($\angle HOH$, °), the angle of the X–H···Y hydrogen bond ($\angle H_O···O$, °), the length of the covalent OH bond, which is not involved in the formation of the hydrogen bond (O–H, Å), the length of the covalent OH bond involved in the formation of the hydrogen bond (O–H$_b$, Å), and the length of the hydrogen bond (O···H$_O$, Å) are calculated. All calculated values are presented in Table 4. The change in the value of a particular structural parameter upon the matrix embedment of the cluster is shown in parentheses next to the value obtained from the geometry optimization of the cluster in a vacuum.

As can be seen from Table 4, the matrix environment affects the structural parameters of the embedded water clusters. For all the considered structures of the water clusters in the matrix, there is a decrease in the $\angle HOH$ angle. For all structures, the lengths of the covalent OH bonds both involved and not involved in the formation of the hydrogen bond remain almost unchanged (the deviations are within 1 %). The magnitude of the hydrogen-bond angle also decreases under the influence of the matrix environment for all structures, except the cyclic pentamer. For the water dimer embedded in the argon crystal, the angle of the hydrogen bond decreases by 3.52°, for the cyclic hexamer by 2.36°, and for the other structures the decrease is within 1°.

The length of the hydrogen bond, as can be seen from Table 4, increases by 2–6 % under the influence of the

Table 4. Change in the values of the structural parameters of water clusters upon embedment in the matrix

Water cluster	$\angle HOH$, °	$\angle O–H···O$, °	O–H, Å	O–H$_b$, Å	O···H$_O$, Å
$H_2O@Ar_{107}$	104.7 (−0.51)	–	0.962 (+0.004)	–	–
$H_2O@Ar_{106}$	104.7 (−0.42)	–	0.962 (+0.001)	–	–
$(H_2O)_2@Ar_{106}$	105.1 (−0.26)	169.7 (−3.52)	0.961 (+0.002)	0.969 (+0.002)	1.940 (+0.062)
$(H_2O)_3@Ar_{105}$	106.0 (−0.21)	150.3 (−0.23)	0.961 (+0.002)	0.975 (+0.0001)	1.890 (+0.054)
$(H_2O)_3@Ar_{104}$	106.0 (−0.10)	150.3 (−0.72)	0.961 (+0.001)	0.975 (−0.0001)	1.890 (+0.051)
$(H_2O)_4@Ar_{104}$	105.7 (−0.29)	167.5 (−0.18)	0.961 (+0.001)	0.982 (−0.001)	1.760 (+0.050)
$(H_2O)_4@Ar_{103}$	105.7 (−0.17)	167.5 (−0.23)	0.961 (+0.001)	0.982 (−0.001)	1.769 (+0.047)
$(H_2O)_5@Ar_{166}$	105.6 (−0.33)	175.6 (+0.65)	0.961 (+0.001)	0.983 (0.001)	1.733 (−0.002)
$(H_2O)_6@Ar_{164}$	105.4 (−0.91)	177.9 (−2.36)	0.961 (+0.002)	0.983 (−0.004)	1.721 (+0.106)

Table 5. The changes of structural parameters of $(H_2O)_6^{cage}$ and $(H_2O)_6^{prism}$ (Å)

Parameter	$(H_2O)_6^{cage}$						
$\Delta(O\cdots H_O)$	O1H12 0.133	O4H15 0.079	O7H5 0.134	O10H9 0.119	O13H2 −0.011	O13H18 0.030	O16H3 0.309
$\Delta(O\text{–}H_b)$	O1H2 0.0	O1H3 −0.003	O4H5 0.0	O7H9 −0.005	O10H12 −0.008	O13H15 −0.003	O16H18 −0.001
Parameter	$(H_2O)_6^{prism}$							
$\Delta(O\cdots H_O)$	O1H5 0.111	O1H9 0.028	O4H11 0.059	O7H6 −0.023	O7H14 0.039	O10H15 −0.065	O10H18 0.183	O13H17 0.021	O16H2 0.041
$\Delta(O\text{–}H_b)$	O1H2 −0.006	O4H5 −0.002	O4H6 0.002	O7H9 −0.0	O10H11 −0.002	O13H14 0.001	O13H15 0.002	O16H17 0.001	O16H18 −0.002

matrix environment. This indicates a weakening of the hydrogen bonds in the clusters embedded in the argon matrix. For a cyclic pentamer, the length of the hydrogen bond decreases by less than 1 %. It should be noted that among the ring structures, the largest elongation of the hydrogen bond in the argon crystal fragment (6.2 %) occurs for the ring hexamer.

For the optimized configurations of three-dimensional hexamer structures, we estimated the changes in the $O\text{–}H_b$ lengths and the lengths of hydrogen bonds that occur in the argon crystal fragment. Each bond is considered separately, as it was not possible to generalize the changes in bond lengths like it was done for the ring structures. The obtained values for two hexamer isomers are presented in Table 5.

As can be seen from Table 5, in the cavities of the matrix, the hydrogen bond strength in hexamer isomers weakens, as evidenced by the increase in the length of the hydrogen bonds in the fragment of the argon crystal. For the two hexamers, $(H_2O)_6^{cage}$ and $(H_2O)_6^{prism}$, both elongation and shortening of the $O\text{–}H_b$ bonds are observed (Table 5). Some changes in the hydrogen bond lengths for prism and cage hexamers are presented in Fig. 4.

The results of the quantum-chemical calculations show that in the simulated $(H_2O)_n@Ar_m$ complexes slight changes in the structural parameters of the water clusters under the influence of the matrix environment are observed. On the one hand, the small values of the deviations in the structures under the influence of the matrix allow for using the matrix isolation method to study the structural and energy characteristics of hydrogen-bonded clusters neglecting their interaction with the environment. On the other hand, even small changes in the of the hydrogen bond length in the clusters cause matrix shifts of vibrational frequencies, which must be taken into account when analyzing the experimental spectra.

3.3. Estimation of matrix shifts for water clusters of different sizes

In vibrational spectra, the effect of the matrix environment on isolated water clusters is manifested in the form of spectral matrix shifts. These are small shifts of the spectral bands relative to the corresponding frequency values for
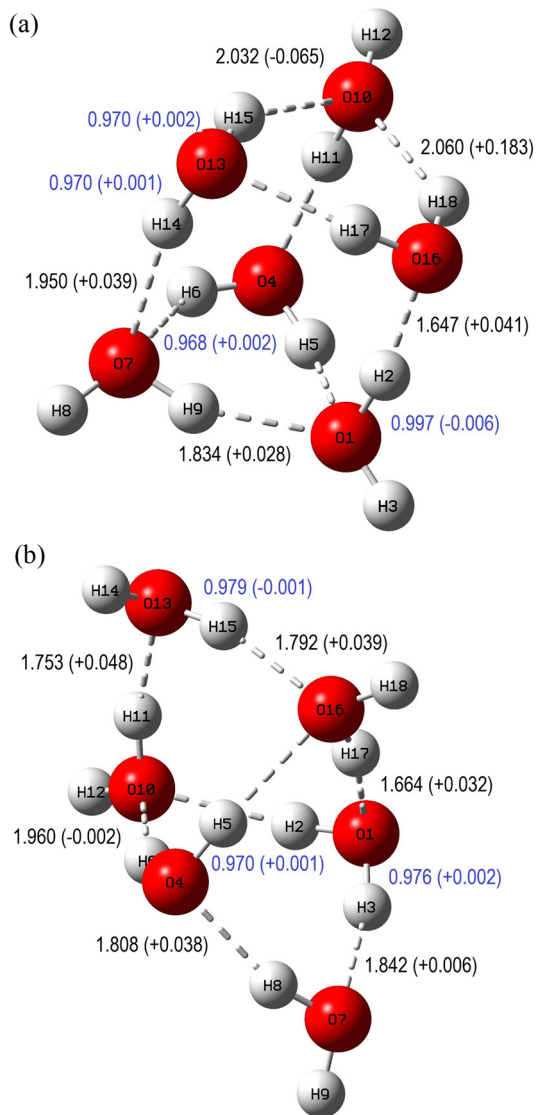

Fig. 4. (Color online) Changes in the length of the $O\cdots H_O$ (black) and $O\text{–}H_b$ bonds (blue) in hexamers of the prism (a) and cage (b) types in the fragment of the argon matrix (Å).

the clusters in a vacuum. The comparison of the matrix shifts obtained in the calculated with the experimentally recorded shifts provides additional information on the possible ways of embedding hydrogen-bonded aggregates in solid-state inert matrices.

Table 6 presents the values of experimentally registered normal vibrational frequencies of the water molecule in the gas phase and in the argon matrix [22]. For each vibrational frequency, the magnitude of the matrix shift (Δ, cm^{-1}) is estimated. The bands in the region of the antisymmetric (ν_{as}) and symmetric (ν_s) OH stretching vibrations in the matrix in comparison with the gas phase redshift by 21.7 and 18.3 cm^{-1}, respectively. For the bending vibration (δ), the matrix shift is about 6 cm^{-1}. A match of the calculated matrix shifts for the complex with the experimental shifts may provide affirmation of a certain form of embedding of the complex in the matrix.

To determine the scaling factors, we compare the IR frequencies for the water monomer calculated using the M06-2X/aug-cc-pVDZ method with those experimentally recorded for water in the gas phase [22]. The value of the scaling factor for a particular vibration is obtained as the ratio of the experimentally-recorded and calculated vibrational frequencies (see Table 7). As can be estimated from the data shown in Table 7, the average value of the scaling factor for the M06-2X-calculated frequencies is about 0.96. This means that the use of the harmonic approximation in the M06-2X frequency calculations overestimates the vibrational frequencies in average by 4 %.

The calculated IR spectra of water clusters are scaled using the determined scaling factors. In Table 8 we show the positions of the bands in the calculated IR absorption spectra of the water monomer and dimer in a vacuum and embedded in a fragment of an argon crystal, as well as the estimated shifts of the corresponding vibrational frequencies. According to the results of the calculations, the bands of the stretching OH vibrations of the water molecule embedded in the fragment of the argon matrix redshift.

Table 6. Comparison of the experimentally registered fundamental vibrational frequencies of a water molecule in the gas phase and in the Ar matrix [22]

Frequency	Gas IR (exp.)	Ar IR (exp.)	Δ, cm^{-1}
ν_s, cm^{-1}	3656.7	3638.4	−18.3
δ, cm^{-1}	1594.6	1588.7	−5.9
ν_{as}, cm^{-1}	3755.8	3734.1	−21.7

Table 7. Comparison of the gas-phase experimental vibrational frequencies of the water molecule with the frequencies calculated using the DFT/M06-2X method

Frequency	Gas IR (exp.) [22]	H$_2$O (DFT/M06-2X)	sf
ν_s, cm^{-1}	3656.7	3860.8	0.9471
δ, cm^{-1}	1594.6	1615.8	0.9869
ν_{as}, cm^{-1}	3755.8	3970.7	0.9459

Table 8. The calculated matrix shifts of vibrational bands for H$_2$O@Ar$_{107}$, H$_2$O@Ar$_{106}$, and (H$_2$O)$_2$@Ar$_{106}$. D_A and D_D denote proton acceptor and donor, respectively

Frequency		H$_2$O	H$_2$O@Ar$_{107}$	$\Delta\nu$, см$^{-1}$
ν_s, см$^{-1}$		3656.7	3617.6	−39.1
δ, см$^{-1}$		1594.6	1595.5	0.9
ν_{as}, см$^{-1}$		3755.8	3712.2	−43.6
		H$_2$O	H$_2$O@Ar$_{106}$	$\Delta\nu$, см$^{-1}$
ν_s, см$^{-1}$		3656.8	3649.6	−7.1
δ, см$^{-1}$		1594.6	1589.2	−5.4
ν_{as}, см$^{-1}$		3755.8	3742.0	−13.8
		(H$_2$O)$_2$	(H$_2$O)$_2$@Ar$_{106}$	$\Delta\nu$, см$^{-1}$
ν_s, см$^{-1}$	D_A	3649.5	3624.1	−25.5
	D_D	3569.9	3546.1	−23.8
δ, см$^{-1}$	D_D	1608.8	1600.0	−8.8
	D_A	1592.0	1578.6	−13.3
ν_{as}, см$^{-1}$	D_A	3745.0	3715.1	−29, 8
	D_D	3730.7	3710.0	−20.8

For the water monomer isolated in an argon crystal, we consider two complexes, and H$_2$O@Ar$_{107}$ is found more energetically stable (see Table 2). The calculated matrix spectral shifts better agree with the experimental data for the H$_2$O@Ar$_{106}$ complex, i.e., the shifts determined for the complex structure where the water monomer replaces two argon atoms. As can be seen in Table 8, the matrix shifts for the symmetric and antisymmetric stretching vibrations of the OH group in H$_2$O@Ar$_{106}$ are 7.1 and 13.8 cm^{-1}, respectively, and the bending-vibration shift is 5.4 cm^{-1}. Thus, for the water monomer embedded into an argon crystal, it can be concluded that the formation of the H$_2$O@Ar$_{107}$ and H$_2$O@Ar$_{106}$ complexes is possible and their ratio likely depends on the water concentration in the matrix.

For the water dimer, the calculated matrix shifts for the symmetric and antisymmetric stretching vibrations are close to the experimental shifts and they are approximately 25 cm^{-1} for both cases (see Table 8). For the bending vibrations, the calculated matrix redshifts for the proton acceptor and proton donor are 13.3 and 8.8 cm^{-1}, respectively. Thus, we can conclude that the embedment of a water dimer into the argon matrix fragment that involves the replacement of two argon atoms in the fragment is quite possible, as evidenced by the formation and deformation energies, as well as by a good match of the calculated matrix shifts and the experiment shifts.

According to the results of the energy calculations (Table 2), the most energetically stable trimer structure is (H$_2$O)$_3$@Ar$_{104}$. The energies of the (H$_2$O)$_3$@Ar$_{105}$ complexes are quite close to the energies of the (H$_2$O)$_3$@Ar$_{104}$ complexes. Thus, a comparison of the calculated and experimental matrix frequency shifts is needed to determine which complex is present in the matrix. The estimated values of the spectral shifts for the (H$_2$O)$_3$@Ar$_{105}$ and (H$_2$O)$_3$@Ar$_{104}$

Table 9. Calculated matrix frequency shifts for $(H_2O)_3@Ar_{105}$ and $(H_2O)_3@Ar_{104}$

Frequency	$(H_2O)_3$	$(H_2O)_3@Ar_{105}$	$\Delta\nu$, см$^{-1}$
ν_s, см$^{-1}$	3457.3	3448.9	−8.5
	3507.4	3494.8	−12.6
	3511.4	3503.1	−8.2
δ, см$^{-1}$	1600.4	1587.9	−12.5
	1601.7	1594.5	−7.2
	1628.9	1619.1	−9.8
ν_{as}, см$^{-1}$	3729.0	3698.1	−30.8
	3729.5	3699.6	−30.0
	3731.7	3703.2	−28.5
	$(H_2O)_3$	$(H_2O)_3@Ar_{104}$	$\Delta\nu$, см$^{-1}$
ν_s, см$^{-1}$	3457.3	3448.8	−8.5
	3508.2	3495.0	−13.1
	3510.2	3506.3	−3.9
δ, см$^{-1}$	1600.5	1580.6	−19.8
	1601.0	1591.0	−10.0
	1628.3	1613.9	−14.4
ν_{as}, см$^{-1}$	3729.3	3699.9	−29.4
	3729.7	3705.5	−24.2
	3731.1	3711.6	−19.5

complexes are presented in Table 9. As it is seen in Table 9, the calculated matrix shifts for the vibrational frequencies in the region of the stretching vibrations are almost the same for the $(H_2O)_3@Ar_{105}$ and $(H_2O)_3@Ar_{104}$ complexes. The average matrix shifts for the symmetric and antisymmetric stretching vibrations of the OH groups in $(H_2O)_3@Ar_{105}$ are 9.8 and 29.8 cm^{-1}, respectively, and for the bending vibrations they are about 9.8 cm^{-1}. In comparison, the average matrix shifts for the $(H_2O)_3@Ar_{104}$ are $\nu_s = 8.5$ cm^{-1} and $\nu_{as} = 24.4$ cm^{-1}, and 14.7 cm^{-1} for the bending vibration. According to the results of the calculations of the formation and deformation energy, $(H_2O)_3@Ar_{105}$ is a more energetically stable complex. The analysis of the matrix shifts of the experimental vibrational frequencies shows similar matrix shifts as those obtained in the calculations (Table 6).

4. Conclusions

Computer simulations of argon fcc crystal fragments with embedded water clusters of different sizes are performed using the DFT/M06-2X quantum-chemical method. The influence of the matrix environment on the structure, energy and spectral properties of individual water clusters is investigated. The formation energies of the $(H_2O)_n@Ar_m$ ($n = 1$–7) complexes, as well as the deformation energies of the embedded water clusters and the argon fragments involved in the embedment are determined in the calculations. The IR matrix spectral shifts of the characteristic water vibrational frequencies occurring in the matrix-isolated water clusters are also calculated. The structures and the embedment me-

chanisms of the water complexes into argon matrices are inferred from the comparison of the calculated vibrational spectra of the complexes and the experimental IR spectra. The best agreement between the calculated and experimental spectra is obtained for the water complexes whose incorporation into the matrix causes minimal disturbance of the argon-crystal structure.

———

1. J. Ceponkus, P. Uvdal, and B. Nelander, *J. Chem. Phys.* **138**, 244305 (2013).
2. J. Ceponkus, P. Uvdal, and B. Nelander, *J. Phys. Chem. A* **116**, 4842 (2012).
3. A. Nemukhin, *Soros Educ. J* **7**, 27 (2000).
4. S. G. Stepanian, A. Y. Ivanov, and L. Adamowicz, *Fiz. Nizk. Temp.* **42**, 1492 (2016) [*Low Temp. Phys.* **42**, 1167 (2016)].
5. V. Y. Pogorelov and I. Y. Doroshenko, *Fiz. Nizk. Temp*. **42**, 1487 (2016) [*Low Temp. Phys.* **42**, 1163 (2016)].
6. A. Vasylieva, I. Doroshenko, O. Doroshenko, and V. Pogorelov, *Fiz. Nizk. Temp.* **45**, 736 (2019) [*Low Temp. Phys.* **45**, 627 (2019)].
7. V. Pogorelov, I. Doroshenko, G. Pitsevich, V. Balevicius, V. Sablinskas, B. Krivenko, and L. G. M. Pettersson, *J. Mol. Liq.* **235**, 7 (2017).
8. K. Kristinaitytė, L. Dagys, J. Kausteklis, V. Klimavicius, I. Doroshenko, V. Pogorelov, N. R. Valevičienė, and V. Balevicius, *J. Mol. Liq.* **235**, 1 (2017).
9. G. Pitsevich, I. Doroshenko, I. Malevich, E. Shalamberidze, V. Sapeshko, V. Pogorelov, and L. G. M. Pettersson, *Spectrochim. Acta A: Mol. Biomol. Spectrosc.* **172**, 83 (2017).
10. S. G. Stepanian and L. Adamowicz, *Fiz. Nizk. Temp.* **46**, 192 (2020) [*Low Temp. Phys.* **46**, 155 (2020)].
11. A. Simon, C. Iftner, and F. Spiegelman, *J. Phys. Chem. A* **119**, 2449 (2015).
12. S. G. Stepanian, A. Y. Ivanov, and L. Adamowicz, *J. Mol. Spectrosc.* **320**, 13 (2016).
13. V. V. Moskva, *Soros Educ. J* **2**, 58 (1999).
14. A. M. Plokhotnichenko, S. G. Stepanian, V. A. Karachevtsev, and L. Adamowicz, *Fiz. Nizk. Temp.* **32**, 201 (2006) [*Low Temp. Phys.* **32**, 148 (2006).
15. A. M. Plokhotnichenko, E. D. Radchenko, Y. P. Blagoĭ, and V. A. Karachevtsev, *Fiz. Nizk. Temp.* **27**, 901 (2001) [*Low Temp. Phys.* **27**, 666 (2001).
16. Y. Zhao and D. G. Truhlar, *Theor. Chem. Accounts* **120**, 215 (2008).
17. L. F. Pacios and P. A. Christiansen, *J. Chem. Phys.* **82**, 2664 (1985).
18. M. M. Hurley, L. F. Pacios, P. A. Christiansen, R. B. Ross, and W. C. Ermler, *J. Chem. Phys.* **84**, 6840 (1986).

19. L. A. LaJohn, P. A. Christiansen, R. B. Ross, T. Atashroo, and W. C. Ermler, *J. Chem. Phys.* **87**, 2812 (1987).

20. M. J. Frisch, G. W. Trucks, H. E. Schlegel, *et al.*, *Gaussian* **16**, Gaussian, Inc., Wallingford CT (2016).

21. S. F. Boys and F. Bernardi, *Mol. Phys.* **19**, 553 (1970).

22. J. Ceponkus, G. Karlström, and B. Nelander, *J. Phys. Chem. A* **109**, 7859 (2005).

Вплив низькотемпературної аргонової матриці
на вбудовані кластери води.
Теоретичне DFT-дослідження

A. Vasylieva, I. Doroshenko, S. Stepanian,
L. Adamowicz

За допомогою квантово-механічного методу DFT/M06-2X проведено моделювання фрагмента ГЦК кристала аргону із вбудованими кластерами води різних розмірів. Досліджено вплив аргонової матриці на структурні, енергетичні та спектральні особливості окремих кластерів води. Розраховано енергії утворення комплексів $(H_2O)_n$@Ar_m ($n = 1$–7), а також енергії деформації кластерів води та кристала аргону. Проведено оцінку матричних зсувів коливальних частот в експериментально зареєстрованих ІЧ спектрах кластерів води, вбудованих в матрицю аргону. Отримані результати дозволили визначити можливість утворення стабільних малих водних комплексів у низькотемпературних матрицях аргону.

Ключові слова: ІЧ спектроскопія, низькотемпературна матрична ізоляція, аргон, кластери води, розрахунки DFT/M06-2X.